4-1993

Photodetachment Cross Section of H- in Crossed Electric and Magnetic Fields. I. Closed-Orbit Theory

Aaron D. Peters
William & Mary

John B. Delos
William & Mary, jbdelo@wm.edu

Recommended Citation

Peters, Aaron D. and Delos, John B., Photodetachment Cross Section of H- in Crossed Electric and Magnetic Fields. I. Closed-Orbit Theory (1993). *Physical Review A*, 47(4), 3020-3035. https://doi.org/10.1103/PhysRevA.47.3020

Photodetachment cross section of H^- in crossed electric and magnetic fields. I. Closed-orbit theory

Aaron D. Peters* and John B. Delos†
Department of Physics, College of William and Mary, Williamsburg, Virginia 23185
(Received 27 August 1992)

In this, the first of two papers, we obtain a simple analytic formula for the photodetachment cross section of H^- in crossed electric and magnetic fields. The three-dimensional semiclassical approximation predicts oscillations in the spectrum and these oscillations are correlated with closed classical orbits. In the following paper [A. D. Peters and J. B. Delos, Phys. Rev. A **47**, 3036 (1993)] we derive fully-quantum-mechanical formulas for the cross section in perpendicular electric and magnetic fields and show how these results can be reduced to the semiclassical results of this paper.

PACS number(s): 32.80.Fb, 03.65.Sq

I. INTRODUCTION

In the past few years much theoretical and experimental work has been conducted in an effort to understand photodetachment of electrons from negative ions, as well as photoionization of atoms in strong static electric and magnetic fields. Garton and Tomkins [1] were the first to observe oscillations in the photoionization cross section near threshold. More detailed experimental work was conducted on the hydrogen atom in a magnetic field [2], and the closed-orbit theory describing these oscillations was given by Du and Delos [3]. A fairly complete quantum-mechanical explanation of these oscillations in various systems has been discussed by several authors [4]. Experimental measurements of the cross section for photodetachment from H^- in strong static electric fields were reported by Bryant *et al.* [5], confirming theoretical predictions made by a number of workers [6]. Especially large oscillations in parallel electric and magnetic fields were predicted by Du [7]. Fabrikant [8] predicted that oscillations would also occur in the photodetachment cross section in crossed electric and magnetic fields. His quantum formulation gives precise numerical predictions, but it does not display the underlying simplicity and order of the oscillations.

In Sec. II we derive a general formula for the photodetachment cross section of H^- in crossed electric and magnetic fields using a three-dimensional semiclassical approximation. We find that the cross section is a smooth background (equal to the no-field photodetachment cross section σ_0) plus a sum of sinusoidal fluctuations. Each oscillation is correlated with an electron orbit that returns to the atom: every returning orbit produces its own sinusoidal oscillation, and when these individual contributions are added together they give the predicted oscillations in the spectrum.

The physical process can be described in the following terms. The active electron is initially in a loosely bound s state of the ion. When the ion absorbs a photon, the electron goes into an outgoing p wave. This wave then propagates away from the neutral hydrogen atom in all directions. Sufficiently far from the atom, the wave propagates according to semiclassical mechanics, and it is correlated with classical trajectories. A pencil of trajectories emanating from a small circular arc about the nucleus is shown in Fig. 1. The wave fronts are transverse to the trajectories, and the waves propagate along the trajectories. Eventually, the trajectories are turned back by the laboratory fields; some of the orbits return to the hydrogen atom, and the associated waves (now incoming) propagate inward until they overlap with the initial state. It is the interference of these returning waves with the steadily produced outgoing waves that leads to the predicted oscillations in the absorption spectrum.

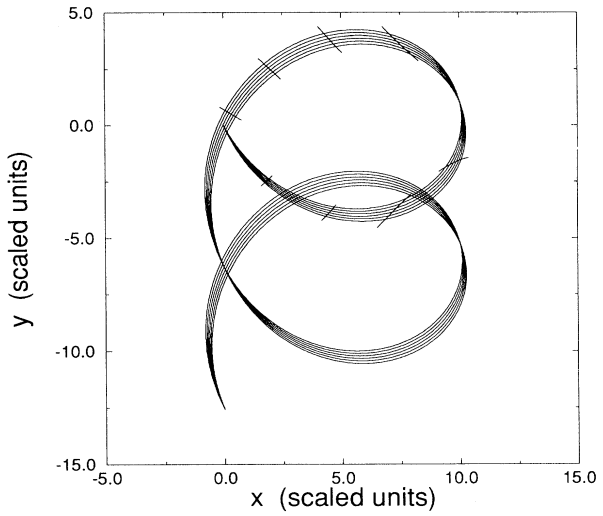

FIG. 1. A pencil of trajectories representing electrons propagating away from the H atom. As the trajectories leave the origin, they diverge from each other, and the probability density is spread out over a larger area. At the caustic, the trajectories cross back over each other and then, after being turned back by the fields, pass close to the atom. The trajectories continue until they pass through a focus, at $t=1$ cyclotron time, where they converge. The process repeats itself. Wave fronts associated with this pencil of trajectories are also drawn. Usually wavefronts are orthogonal to trajectories but not in a magnetic field.

In Sec. III we analyze the returning orbits for the case of perpendicular electric and magnetic fields. Consistent with the order of the trajectories visible in Fig. 1, the set of returning orbits has an orderly pattern: at the lowest energies there is one returning orbit, and at each of a set of "boundary energies" two additional returning orbits are created. The important properties of each trajectory are the following: (i) its classical action, which determines the phase of the returning wave relative to the outgoing wave; (ii) its Maslov index, which counts the number of caustics and foci through which the trajectory passes, and gives corrections to the classical phase; and (iii) the classical density of the neighbors of each returning trajectory, which determines the amplitude of each returning wave.

Quantitative formulas for the action, Maslov index, and classical density associated with each closed orbit are presented in Sec. III. Additionally, a quantitative formula for the boundary energies is provided.

In Sec. IV the general expression for the semiclassical photodetachment cross section, which was derived in Sec. II, is evaluated using the classical results of Sec. III. A simple and lovely pattern of oscillations is displayed. The oscillations are small, but they may be detectable close to the threshold.

Presently no experiments on photodetachment in crossed fields have been carried out. Our predictions show that there are interesting phenomena here, and we hope that our calculations may guide future measurements.

II. THE PHOTODETACHMENT CROSS SECTION

We treat photodetachment as a one-electron process. We imagine that there is a short-range, spherically symmetric potential $V_b(r)$ which loosely binds the active electron to the hydrogen atom. The most important fact about the applied electric and magnetic fields is that they are weak in atomic units. Therefore, although they greatly affect the large-scale motion of the electron, they have a negligible effect on the motion at small scales. On an atomic length scale, the electron moves on a straight line at constant speed.

The energy of the detached electron is denoted by E. The binding energy of the electron to the negative ion is $E_b=\hbar^2k_b^2/2m_e$, where E_b is approximately 0.754 eV and the mass of the electron is denoted by m_e. The photon energy is expressed as $E_p=E_b+E$. The photodetachment cross section is related to an oscillator-strength density $Df(E)$ in the following way:

$$\sigma=\frac{2\pi^2}{m_e c}e^2\hbar Df(E) . \tag{2.1}$$

It has been shown by Du and Delos [3] that the oscillator-strength density can be expressed as

$$Df(E)=-\frac{2m_eE_p}{\pi\hbar^2}\mathrm{Im}\langle D\Psi_i|\hat{G}^+|D\Psi_i\rangle . \tag{2.2}$$

The outgoing Green's function is denoted by $\hat{G}^+$. The dipole operator D is equal to the projection of the electron coordinate onto the direction of polarization of the laser field.

Our previously discussed physical picture develops out of this formula. The initial state $|\Psi_i\rangle$ is modified by the dipole operator associated with the laser field to give a "source function" $|D\Psi_i\rangle$. The Green's function $\hat{G}^+$ propagates these waves outward at fixed energy within the "atomic" region, near the atomic core. At $(5-10)a_0$ this quantum wave is joined to a semiclassical wave, which propagates along trajectories. The trajectories are turned around by the laboratory fields, and some are returned to the origin. At around $10a_0$ the returning semiclassical wave is very nearly a plane wave, and so we join it to a quantum-mechanical plane wave, which we expand in partial waves. Finally, the incoming waves overlap with $\langle D\Psi_i|$, giving the interference pattern in the absorption spectrum.

The final result is that the photodetachment cross section is given by the formula

$$\sigma_q=\sigma_0+\sum_j C_j(E)\sin\Phi_j(E) , \tag{2.3}$$

where the summation is over all closed orbits. σ_0 is the no-field cross section. The phase $\Phi_j(E)$ of the sinusoidal oscillations is given by

$$\Phi_j(E)=-S_j(E)/\hbar+\mu_j\frac{\pi}{2} . \tag{2.4}$$

$S_j(E)$ is the classical action for the returning orbit evaluated at its return time t_{ret}. The returning orbit passes through caustics and foci on its way back to the origin. At each such "singular point" the phase undergoes a change of $\pi/2$. The Maslov index (μ_j) is equal to the total number of singular points through which the electron passes on its journey. The action, Maslov index, and phase are independent of the direction of polarization.

The amplitude of each oscillation $C_j(E)$ is given by

$$C_j(E)=\frac{16\pi^2}{c}\frac{e^2}{\hbar}\frac{2m_eE_p}{\hbar^2}\frac{1}{r_{\mathrm{out}}}\left|\frac{J_j(t_0)}{J_j(t_{\mathrm{ret}})}\right|^{1/2} I_{l=1}^2 \times[\chi(\theta^j_{\mathrm{out}},\phi^j_{\mathrm{out}})\chi^*(\theta^j_{\mathrm{ret}},\phi^j_{\mathrm{ret}})] . \tag{2.5}$$

We call this quantity the "recurrence amplitude." This formula contains "classical" factors, related to the orbits, and "quantum" factors, related to the initial atomic state and dipole operator. The factor $I_{l=1}$ appearing in Eq. (2.5) is a radial dipole integral between the initial state (presumed to be an s state) and the outgoing wave state (which therefore must be p). It determines the overall magnitude of the detachment cross section and of the oscillations. $\chi(\theta,\phi)$ is the angular distribution of outgoing waves (p_x or p_y in our case, according to the polarization vector of the laser field). The angles $\{\theta^j_{\mathrm{out}},\phi^j_{\mathrm{out}}\}$ and $\{\theta^j_{\mathrm{ret}},\phi^j_{\mathrm{ret}}\}$ refer to the outgoing and returning directions of the jth closed orbit. Finally, $(1/r^2_{\mathrm{out}})|J_j(t_0)/J_j(t_{\mathrm{ret}})|$ is the classical density of the returning wave.

The reader may recall that a similar formula was obtained in Ref. [3] for photoionization of atoms in a magnetic field. The present formula differs from that one in two important ways: (i) For ionization, there is a long-

range Coulomb force which substantially modifies the outgoing waves. In Ref. [3], the dipole integral involved zero-energy Coulomb waves, and hiding in the formula was a Coulomb density of states. In the present case, a free-particle approximation can be used for the outgoing waves near the atom. (ii) In a magnetic field only, the forces are cylindrically symmetric. Therefore, in Ref. [3], each returning orbit actually represents a cylindrical family of orbits, having initial azimuthal angles between 0 and 2π. In crossed fields, this symmetry does not hold, so each returning orbit is isolated. As a consequence, much smaller oscillations are obtained in the present case.

The remainder of this section gives the proof of Eqs. (2.3)–(2.5). The reader may prefer to skip to Sec. III, where returning orbits are presented.

A. The Hamiltonian, initial wave function, and dipole operator

The Hamiltonian is given by

$$H=\frac{1}{2m_e}\left[\mathbf{p}+\frac{e}{c}\mathbf{A}\right]^2-eV\ , \tag{2.6}$$

where e is the absolute value of the electron charge. In the particular case of perpendicular fields (with H_0 pointing in the $+z$ direction and F in the $+x$ direction), we may choose the potentials in the following way:

$$\begin{aligned}&\mathbf{A}=H_0 x\hat{\mathbf{y}}\ ,\\ &V=-Fx+V_b(r)\ ,\end{aligned} \tag{2.7}$$

where $V_b(r)$ is the effective potential that binds the active electron to the form. Then the Hamiltonian has the following form:

$$\begin{aligned}H=&\frac{1}{2m_e}p_x^2+\tfrac{1}{2}m_e\omega_B^2\left[x+\frac{p_y}{m_e\omega_B}\right]^2\\ &+eFx+\frac{1}{2m_e}p_z^2-eV_b(r)\ ,\end{aligned} \tag{2.8}$$

where the electron cyclotron frequency is given by

$$\omega_B=\frac{eH_0}{m_e c}\ . \tag{2.9}$$

For the development in this section, there is only one important property of the Hamiltonian: if r is sufficiently small, and the applied fields are weak compared to $V_b(r)$, then the terms proportional to F and to ω_B can be neglected. The Hamiltonian reduces to that of an electron interacting with a short-range potential energy.

For the bound state we can use a familiar approximation, which has been found in the past to be quite accurate:

$$\Psi(\mathbf{r})=B_0\frac{e^{-k_b r}}{r}\equiv\frac{R(r)}{\sqrt{4\pi}}\ . \tag{2.10}$$

B_0 is a "normalization" constant, which must be chosen with care; the appropriate value is 0.315 52 in a.u. The constant k_b is related to the binding energy of the active electron $E_b=\hbar^2k_b^2/2m_e$.

When a dipole operator ($D=a_x x+a_y y+a_z z$) acts on these states it produces a p state, or combination of p states:

$$|D\Psi_i\rangle=rR(r)\chi(\theta,\phi)\ . \tag{2.11}$$

Since the initial state is spherically symmetric and we assume that the light is linearly polarized, the angular factors are single p waves:

$$\begin{aligned}\chi_x(\theta,\phi)&=\frac{1}{\sqrt{4\pi}}\sin\theta\cos\phi\ ,\\ \chi_y(\theta,\phi)&=\frac{1}{\sqrt{4\pi}}\sin\theta\sin\phi\ ,\\ \chi_z(\theta,\phi)&=\frac{1}{\sqrt{4\pi}}\cos\theta\ .\end{aligned} \tag{2.12}$$

B. The Green's function, outgoing waves, and the direct contribution to the cross section

When the laser photodetaches the electron, outgoing electron waves are produced. The Green's function $G^+(\mathbf{q},\mathbf{q}';E)$ represents the waves at $\mathbf{q}$ which arise from a source at $\mathbf{q}'$. Since in Eq. (2.2) the Green's function sits between $\langle D\Psi_i|$ and $|D\Psi_i\rangle$, the relevant source points $\mathbf{q}'$ and the field points $\mathbf{q}$ all lie within a few bohrs of the nucleus. Two types of waves arrive at $\mathbf{q}$. First, there are waves which propagate outward from $\mathbf{q}'$ to $\mathbf{q}$ without ever leaving the vicinity of the nucleus. Second, there are waves that propagate outward from $\mathbf{q}'$, travel into the external region, are turned around by the perpendicular electric and magnetic fields, and return to the vicinity of the nucleus, finally arriving at $\mathbf{q}$. The distinction between the two types is unambiguous; therefore

$$G^+(\mathbf{q},\mathbf{q}';E)=G^+_{\rm dir}(\mathbf{q},\mathbf{q}';E)+G^+_{\rm ret}(\mathbf{q},\mathbf{q}';E)\ . \tag{2.13}$$

First let us consider the direct term. For $\mathbf{q}$ somewhat larger than $\mathbf{q}'$, the quantity $G^+_{\rm dir}|D\Psi_i\rangle$ represents outgoing electron waves. The binding potential has a short range, and the waves quickly propagate outside the influence of the atom and through a region ($3a_0\le r\le 10a_0$) where neither the atomic potential nor the applied fields have any significant effect. We conclude, therefore, that the Green's function which propagates these waves is the Green's function of a free particle

$$G^+=\sum_{l,m}g_l^E(r,r')Y_{l,m}(\theta,\phi)Y^*_{l,m}(\theta',\phi')\ , \tag{2.14}$$

where

$$g_l^E(r,r')=\left[\frac{-2im_e}{\hbar^2}\right]kj_l(kr_<)h_l^+(kr_>)\ . \tag{2.15}$$

The standard notation that $r_>=\max\{r,r'\}$ and $r_<=\min\{r,r'\}$ has been used. From this we can get an explicit expression for the outgoing waves. Defining

$$I_l(k)=\int_0^\infty j_l(kr')r'^3R(r')dr'\ , \tag{2.16}$$

where we obtain for the integral [9]

$$I_{l=1}(k)=B_0\sqrt{4\pi}\frac{2k}{(k_b^2+k^2)^2}\ , \tag{2.17}$$

the outgoing wave can be expressed as

$$\hat{G}^{+}|D\Psi_i\rangle=\frac{-2im_e}{\hbar^2}kh_1^{+}(kr)I_{l=1}(k)\chi(\theta,\phi)\ . \quad (2.18)$$

Its amplitude is proportional to the radial dipole integral $I_{l=1}$, and its angular distribution is given by $\chi(\theta,\phi)$.

With this, we can evaluate the contribution of $G^{+}_{\rm dir}$ to the photodetachment cross section:

$$\sigma_{\rm dir}=\frac{-2\pi}{c}\frac{e^2}{\hbar}2E_p{\rm Im}\langle D\Psi_i|\hat{G}^{+}_{\rm dir}|D\Psi_i\rangle\ . \quad (2.19)$$

Using Eq. (2.18) we find

$$\sigma_{\rm dir}=\frac{64\pi^2}{3c}B_0^2\frac{k^3}{(k_b^2+k^2)^3}\frac{e^2}{\hbar}=\sigma_0\ . \quad (2.20)$$

Since the external fields only affect the large-scale motion of the electron, the direct contribution to the cross section is the same as if there were no fields present.

C. Returning waves and spectral oscillations

In this section we will calculate the returning waves

$$\Psi_{\rm ret}=\hat{G}^{+}_{\rm ret}|D\Psi_i\rangle \quad (2.21)$$

and their contribution to the photodetachment cross section

$$\sigma_{\rm ret}=\frac{-2\pi}{c}\frac{e^2}{\hbar}2E_p{\rm Im}\langle D\Psi_i|\Psi_{\rm ret}\rangle\ . \quad (2.22)$$

To calculate $\Psi_{\rm ret}(\mathbf{r})$ the following reasoning is used. $\hat{G}^{+}_{\rm dir}|D\Psi_i\rangle$ is a wave that propagates outward from the atomic core where $|D\Psi_i\rangle$ is substantial. Anywhere between $5a_0$ and $10a_0$ these outgoing waves are joined to semiclassical waves on a sphere. The semiclassical waves are correlated with trajectories, and with each trajectory that returns to the sphere there is an associated returning semiclassical wave function. Only returning trajectories and their associated waves can form a substantial overlap with $\langle D\Psi_i|$. Near the atomic core the returning semiclassical wave function is proportional to a quantum-mechanical plane wave. The two are joined and the quantum-mechanical plane wave continues to propagate inward to overlap with $\langle D\Psi_i|$. Thus a returning wave is associated with each closed orbit, and the full returning wave $\Psi_{\rm ret}(\mathbf{r})$ is the sum of such returning waves.

1. The direct part produces an outgoing wave

Equation (2.18) gave an expression for the outgoing wave. At fairly large distances ($kr>3$) we can use the asymptotic approximation for the Hankel function, which is given by

$$h_l^{+}(kr)\simeq(-i)^{l+1}\frac{e^{i\mathbf{k}\cdot\mathbf{r}}}{kr}\ , \quad (2.23)$$

to obtain

$$\hat{G}^{+}_{\rm dir}|D\Psi_i\rangle\simeq\frac{2im_e}{\hbar^2}\frac{1}{r}e^{i\mathbf{k}\cdot\mathbf{r}}I_{l=1}(k)\chi(\theta,\phi)\ . \quad (2.24)$$

2. The outgoing wave is joined to a semiclassical wave, which propagates to large distances

We now wish to continue this wave into the region where the laboratory fields cannot be neglected. This continuation is accomplished with a semiclassical approximation. In order to construct the semiclassical wave function, a two-dimensional surface with two intrinsic coordinates $\mathbf{q}^0$ is defined. We choose a spherical surface centered at the origin with radius $r_{\rm out}\simeq 10a_0$. The spherical angles $\theta_{\rm out}$ and $\phi_{\rm out}$ are chosen as the two coordinates of the surface. Let the outgoing wave $G^{+}_{\rm dir}|D\Psi_i\rangle$ evaluated on this surface be written as

$$\Psi(\mathbf{q}^0)=(\hat{G}^{+}|D\Psi_i\rangle)_{r=r_{\rm out}}=A(\mathbf{q}^0)e^{iS(\mathbf{q}^0)/\hbar}\ . \quad (2.25)$$

Then a semiclassical approximation to the wave $\Psi(\mathbf{q})$ outside the surface is given by

$$\Psi(\mathbf{q})=\sum_j\Psi(\mathbf{q}^0)A_j(\mathbf{q})e^{i[S_j(\mathbf{q})/\hbar-\mu_j\pi/2]}\ , \quad (2.26)$$

where

$$S_j(\mathbf{q})=\int_{q^0}^{q}\mathbf{p}\cdot d\mathbf{q}\ ,$$
$$A_j(\mathbf{q})=\left[\frac{J(t=0,\mathbf{q}_j^0)}{J(t,\mathbf{q}_j^0)}\right]^{1/2}\ , \quad (2.27)$$
$$J(t,\mathbf{q}_j^0)=\left|\det\left[\frac{\partial\mathbf{q}_j(t,\mathbf{q}_j^0)}{\partial(t,\mathbf{q}_j^0)}\right]\right|\ .$$

The integral for $S_j(\mathbf{q})$ is evaluated on a classical trajectory having energy E, emanating from the initial surface at $\mathbf{q}_j^0$ and arriving at $\mathbf{q}$. The sum is over all returning trajectories which arrive at the point $\mathbf{q}$ from different points $\mathbf{q}_j^0$ on the initial surface. The Jacobian $J(t,\mathbf{q}_j^0)$ is evaluated by examining the divergence of adjacent trajectories from each central trajectory going from the point $\mathbf{q}_j^0$ to $\mathbf{q}$. The quantity μ_j in Eq. (2.26) is the Maslov index.

The Maslov index is calculated by counting caustics and foci, which are singular points where $J(q)$ goes to zero and $A(q)$ goes to infinity. These singular points produce additional phase shifts of the wave, and these phase shifts are described by the Maslov index. In the present case the caustics are of the simplest type, known as a "fold" (at which the trajectories curve back over each other, producing a boundary between classically allowed and forbidden regions). As the trajectory passes through the fold, the Maslov index increases by 1, and the wave undergoes a phase loss of $\pi/2$.

There is another type of singular region. At a focus, where trajectories converge from a circle to a point, the Jacobian will also go to zero. Associated with such a focus is also a phase loss of $\pi/2$.

By examining the classical equations of motion it will be possible to determine, for a particular closed orbit, the number of caustics and foci encountered. Combining Eq. (2.26) and the formula (2.24) for the outgoing wave on the initial surface, the wave function in the external region is

$$\Psi(\mathbf{q})=\sum_j \left[\frac{2im_e}{\hbar^2}\frac{1}{r_{\rm out}}e^{i\mathbf{k}^j_{\rm out}\cdot\mathbf{r}_{\rm out}}I_{l=1}(k^j_{\rm out})\chi(\theta^j_{\rm out},\phi^j_{\rm out})\right] \times\left|\frac{J_j(t_0)}{J_j(t)}\right|^{1/2}e^{i[S_j(t)/\hbar-\mu_j\pi/2]} . \quad (2.28)$$

Again the sum is over all trajectories that arrive at $\mathbf{q}$ from the initial surface.

3. The semiclassical wave returns

Each point on the initial sphere with radius $r_{\rm out}$ defines a set of initial conditions for classical trajectories. Integrating the equations of motion, we follow the trajectory through space. Leaving the atomic region, the electron interacts with the laboratory fields and the trajectory is turned around by the fields. Initial conditions giving rise to closed orbits return at various times to the sphere at $r_{\rm ret}$. For each such orbit there is a point on the sphere defined by the coordinates $\{r_{\rm ret},\theta^j_{\rm ret},\phi^j_{\rm ret}\}$, and the kinetic momentum of the returning electron at that point is $m_e\mathbf{v}^j_{\rm ret}\equiv\hbar\mathbf{k}^j_{\rm ret}$.

Around each closed orbit, or central trajectory, there is a family of trajectories which also returns to the sphere at $r_{\rm ret}$. These trajectories stay close to the central trajectory, and the ratio of Jacobians measures the classical density associated with this family of trajectories.

The returning wave function evaluated on the sphere defined by $r_{\rm ret}$ is therefore given by

$$\Psi^j_{\rm ret}(\mathbf{r}_{\rm ret})=\left[\frac{2im_e}{\hbar^2}\frac{1}{r_{\rm out}}e^{i\mathbf{k}^j_{\rm out}\cdot\mathbf{r}_{\rm out}}I_{l=1}(k^j_{\rm out})\chi(\theta^j_{\rm out},\phi^j_{\rm out})\right] \times\left|\frac{J_j(t_0)}{J_j(t_{\rm ret})}\right|^{1/2}e^{i[S_j(t_{\rm ret})/\hbar-\mu_j\pi/2]} . \quad (2.29)$$

Inside this circle the semiclassical waves associated with each returning orbit are approximately equal to plane waves:

$$\Psi^j_{\rm ret}(\mathbf{r})\propto N_j e^{i\mathbf{k}^j_{\rm ret}\cdot\mathbf{r}} , \quad (2.30)$$

where N_j is a normalization factor. It is determined by letting $r\to r_{\rm ret}$:

$$N_j=\left[\frac{2im_e}{\hbar^2}\frac{1}{r_{\rm out}}I_{l=1}(k^j_{\rm out})\chi(\theta^j_{\rm out},\phi^j_{\rm out})\right] \times\left|\frac{J_j(t_0)}{J_j(t_{\rm ret})}\right|^{1/2}e^{i[S_j(t_{\rm ret})/\hbar-\mu_j\pi/2]}\frac{e^{i\mathbf{k}^j_{\rm out}\cdot\mathbf{r}_{\rm out}}}{e^{i\mathbf{k}^j_{\rm ret}\cdot\mathbf{r}_{\rm ret}}} . \quad (2.31)$$

If the approximations we have made are valid, then N_j will be independent of the radius of the final sphere $r_{\rm out}$. In Eq. (2.31) we can conveniently take the limit $r_{\rm out}=r_{\rm ret}\to 0$. In this limit the quantity

$$\frac{1}{r_{\rm out}}\left|\frac{J_j(t_0)}{J_j(t_{\rm ret})}\right|^{1/2} \quad (2.32)$$

approaches a finite value, and $S_j(E)$ becomes the action integral over the full closed orbit, starting and ending at the origin.

4. The returning wave overlaps the initial state

To calculate the overlap of the returning wave with the source function, we use the partial-wave expansion of the returning wave. The expansion of a plane wave, Eq. (2.30), in spherical harmonics is well known:

$$\Psi^j_{\rm ret}(\mathbf{r})=4\pi N_j\sum_{l,m}(i)^l j_l(k^j_{\rm ret}r)Y_{l,m}(\theta,\phi)Y^*_{l,m}(\theta_{k^j_{\rm ret}},\phi_{k^j_{\rm ret}}) , \quad (2.33)$$

where $\{\theta_{k^j_{\rm ret}},\phi_{k^j_{\rm ret}}\}$ are angles defining the direction of $k^j_{\rm ret}$, the direction in which the returning wave is propagating. We would like to express this in terms of the angles $\theta_{\rm ret}$ and $\phi_{\rm ret}$ (the direction from which the returning trajectory comes). Since $\theta_{\rm ret}=\pi-\theta_{k^j_{\rm ret}}$, and $\phi_{\rm ret}=\pi+\phi_{k^j_{\rm ret}}$, we have

$$\Psi^j_{\rm ret}(\mathbf{r})=4\pi N_j\sum_{l,m}(-i)^l j_l(k^j_{\rm ret}r)Y_{l,m}(\theta,\phi) \times Y^*_{l,m}(\theta^j_{\rm ret},\phi^j_{\rm ret}) . \quad (2.34)$$

To get the cross section we only have to find the overlap of this returning wave with $\langle D\Psi_i|$ and sum over all returning waves. The same radial dipole integral, $I_{l=1}$, and angular functions $\chi(\theta,\phi)$ are involved, and so we find

$$\sigma_{\rm ret}=\frac{-16\pi^2}{c}\frac{e^2}{\hbar}\frac{2m_eE_p}{\hbar^2}\sum_j\frac{1}{r_{\rm out}}\left|\frac{J_j(t_0)}{J_j(t_{\rm ret})}\right|^{1/2} I^2_{l=1}[\chi(\theta^j_{\rm out},\phi^j_{\rm out})\chi^*(\theta^j_{\rm ret},\phi^j_{\rm ret})]\sin[S_j(t_{\rm ret})/\hbar-\mu_j\pi/2] . \quad (2.35)$$

Thus we have arrived at Eqs. (2.3)–(2.5).

Up to this point all our work has been of a general nature, i.e., the equations which have been derived are valid for any orientation of the external fields, and for any laser polarization. In the next section we will compute trajectories for perpendicular fields and derive formulas for the action, density, and Maslov indices for returning orbits.

III. THE CLASSICAL MOTION

In this section we examine the trajectories for an electron in perpendicular electric and magnetic fields. As is well known, if the magnetic field (H_0) points in the positive z direction, and the electric field (F) is in the positive x direction, the motion of the electron can be separated

into constant velocity motion along the z axis, and a motion in the x-y plane. For returning orbits p_z must equal zero. Motion in the x-y plane is that of a trochoid: a circular motion about a center superposed upon a translational motion down the y axis. For returning orbits the linear speed must be less than the circular speed.

Calculations show that at low energy (E) there is always one returning orbit. As the energy increases, the trajectories change their shape, and at each of a set of discrete boundary energies a new closed orbit arises. The newly formed orbit separates into a pair with the slightest increase of energy. For any given energy E, other than the boundary energies, there are $(2j+1)$ returning orbits.

In the first part of this section, we will display these facts using pictures of the orbits. In the second part we will give a quantitative analysis, i.e., we will obtain formulas for the classical action, density, and Maslov index. These formulas will subsequently be used to evaluate the photodetachment cross section, derived in Sec. II, for perpendicular electric and magnetic fields.

A. Families of trajectories and returning orbits

Classically, once the electron is photodetached, it will exhibit trochoidal motion: circular cyclotron motion at constant speed relative to a center moving at the fixed "$E\times B$ drift" velocity. This is described in many textbooks [10]. It is convenient to define a set of scaled variables:

$$\mathbf{q}'=m_e\frac{\omega_B^2}{eF}\mathbf{q}\ ,$$
$$t'=\omega_B t\ . \tag{3.1}$$

Units of time are chosen such that one cyclotron period is 2π units, and units of length are chosen such that the drift velocity is 1. In these units, the position as a function of time is

$$x(t)=\sqrt{2\varepsilon}[\sin(t+\varphi)-\sin(\varphi)]\ ,$$
$$y(t)=-\sqrt{2\varepsilon}[\cos(t+\varphi)-\cos(\varphi)]-t\ , \tag{3.2}$$
$$z(t)=p_{z_0}t\ .$$

We recognize these equations to be the parametric representation of a trochoid: circular motion about a center superposed upon a translational motion. The circular motion is primarily due to the interaction of the electron with the magnetic field. The radius of this motion is given by the quantity $\sqrt{2\varepsilon}$, which (since the angular velocity is equal to 1 in scaled units) also represents the speed of the circular motion. ε is that part of the kinetic energy associated with the circular motion. The translation of the electron ("$E\times B$ drift") has a velocity $-eF/m_e\omega_B$; in scaled units it has a fixed value of -1.

If the linear speed exceeds the circular speed ($1>\sqrt{2\varepsilon}$), the trajectory is curtate and never intersects itself. If the linear speed is less than the circular speed, the trajectory is prolate and self-intersecting. When the two are equal it is a cycloid (Fig. 2).

The initial conditions on the trajectories follow from the fact that the electron was detached from an H^- ion by a laser: all electrons begin at $\{x=0,y=0,z=0\}$ going outward in all directions, all at the same speed, determined by the photon energy. Scrutinizing Eq. (3.2) we find that this condition of fixed initial speed implies that there must be a relationship between φ and ε. This implies a relationship between the initial direction of propagation and the radius of the circular motion.

Figure 3 shows the whole family of electron orbits in the x-y plane at low photon energy. In scaled units, the electron's energy is its initial kinetic energy:

$$E'=\frac{1}{2}\left|\frac{d\mathbf{q}'}{dt'}\right|^2_{t=0}\ . \tag{3.3}$$

The orbits in Fig. 3 have $E=1$.

All three types of motion are visible in Fig. 3. There is one self-intersecting prolate orbit that allows the electron to return to the atom. This returning trajectory has been emphasized in the figure. Other things are also visible. The trajectories all focus on a point on the negative y axis after one cyclotron time. The caustics, or boundaries be-

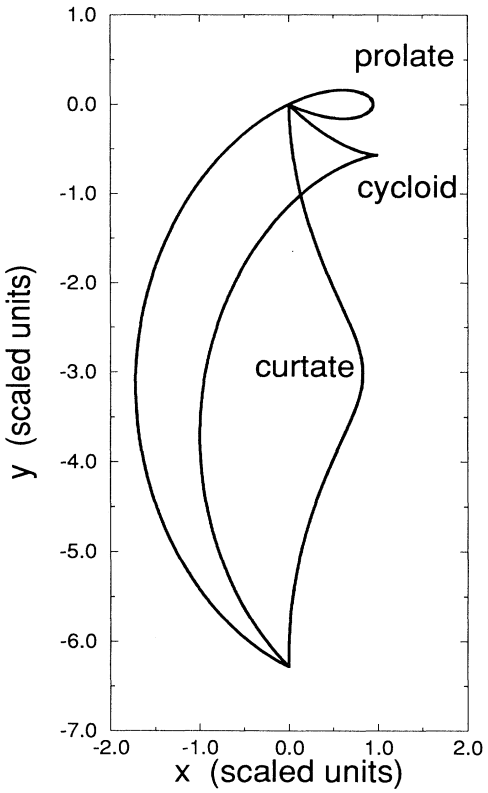

FIG. 2. For any returning orbit, the momentum in the z direction must be zero. The motion of the electron is therefore confined to the x-y plane if there are to be returning orbits. Furthermore, the equations for $x(t)$ and $y(t)$ are the parametric representation of a trochoid. We have circular motion around a center which moves at constant speed down the y axis. If the linear speed exceeds the circular speed ($\sqrt{2\varepsilon}$), the trajectory is curtate. If the circular speed is larger, the trajectory is prolate, and may return to the origin. When they are equal it is a cycloid.

tween classically allowed and forbidden regions, are also apparent.

What happens if the photon energy is increased? The electron begins with a larger kinetic energy, but since the drift velocity is fixed at cF/H_0 (or 1 in scaled units), the increased energy can only go into the circular motion. The circles then have a larger radius and higher speed, so therefore any curtate orbits eventually disappear and the prolate orbits become larger and more tightly wound. This is apparent in Fig. 4. Note that the location of the first caustic is now closer to the origin than in Fig. 3. Again we have emphasized the one returning orbit in the figure.

Increasing the scaled energy to a value $E=E^{(b1)}$, close to 9.5 scaled units (Fig. 5), we find that this caustic now touches the origin, and a new closed orbit has been created. We call this the first boundary energy. Increasing the energy further, the new closed orbit splits into two (Fig. 6).

As we continue to increase the energy, the second caustic on the y axis begins to approach the origin (Fig. 7). At the second boundary energy, $E=E^{(b2)}$, which is approximately 29.5 scaled units, the caustic comes tangent to the origin, and again a new closed orbit is created (Fig. 8). As the caustic rises above the x axis, the newly formed closed orbit than splits into two (Fig. 9). Thus as the energy increases, the closed orbits increase in steady progression from one to three to five, and so on.

B. Returning orbits—quantitative theory

Let us now give a quantitative analysis of returning orbits. The essential results of this section are the following: (i) An approximate formula, Eq. (3.18), for the boundary energies at which new closed orbits appear. (ii) A formula, Eq. (3.25), for the Jacobian, which gives the classical density associated with the trajectories. It therefore will give the amplitude of the returning wave; it will also verify our prescription for the Maslov index. (iii) A formula, Eq. (3.35), for the classical action on an orbit. This determines the phase of the returning wave. The reader who is not interested in the derivation of these formulas may now skip to Sec. IV.

The equations that appear later will be easier to understand if we begin with a preliminary remark. The total energy of the electron is

$$E=\tfrac{1}{2}m_e\mathbf{v}^2+eFx\ , \tag{3.4a}$$

and the drift velocity is in the minus-y direction. Let us define v_y' as the y component of the electron's velocity relative to the drift frame:

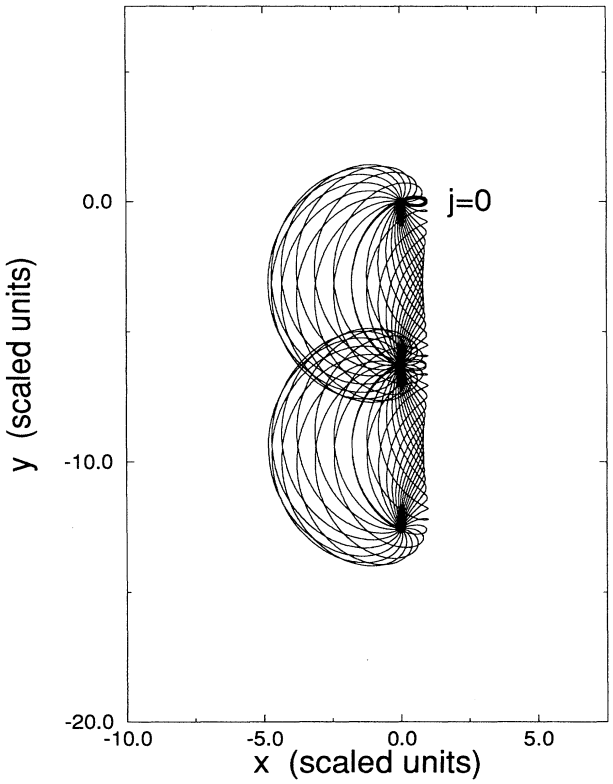

FIG. 3. The entire family of outgoing electron trajectories at a scaled energy $E=1$. There is one closed orbit (bold, "balloon-shaped" curve) which is labeled with $j=0$. Note the boundaries between the classically allowed and classically forbidden regions (caustics). Also, all trajectories focus on a point on the negative y axis after one cyclotron time.

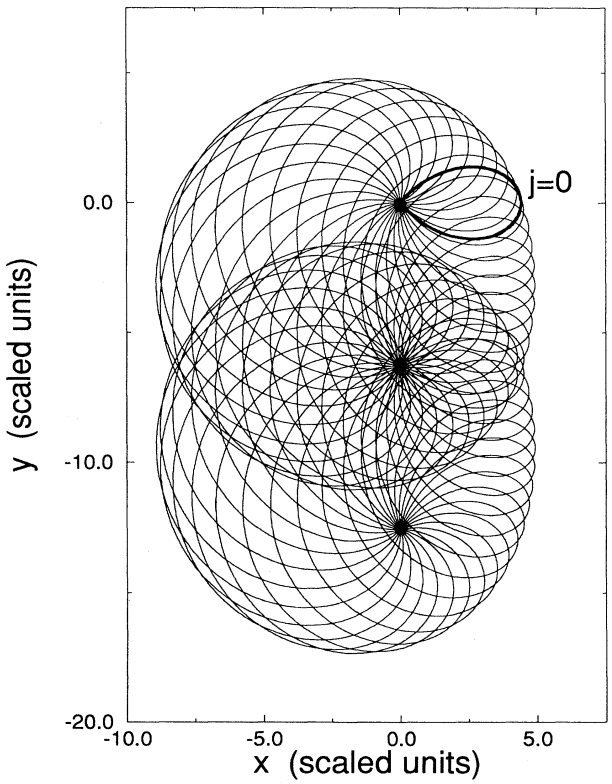

FIG. 4. The total scaled energy E has been increased to 6. The "balloon-shaped" orbit associated with $j=0$ has grown in size and become more circular. The first caustic is approaching the x axis from below.

$$v_y' = v_y + v_d \ , \tag{3.4b}$$

$$v_y'^2 - 2v_y' v_d + v_d^2 = v_y^2 \ . \tag{3.4c}$$

Using Eq. (3.4c), the total energy can be written in the form

$$E = \varepsilon + \tfrac{1}{2} m_e v_z^2 - \tfrac{1}{2} m_e v_d^2 - p_y v_d \ , \tag{3.4d}$$

where

$$\varepsilon \equiv \tfrac{1}{2} m_e (v_x^2 + v_y'^2) \ , \tag{3.4e}$$

$$p_y \equiv m_e (v_y - \omega_B x) \ . \tag{3.4f}$$

Here ε is the kinetic energy of circular motion of the electron, as seen in the drift frame. We know that this is conserved. v_z is also conserved, v_d is a constant, and the total energy is conserved, so it follows that p_y, defined in Eq. (3.4f), must also be conserved. (This says that the x component of position and the y component of velocity oscillate 180° out of phase with each other.) Furthermore, the initial value of p_y is the initial y component of the kinetic momentum, $m_e v_y^0$.

In what follows, we will use these conservation laws to derive the required quantitative properties of the returning orbits. To retain the close connection with quantum

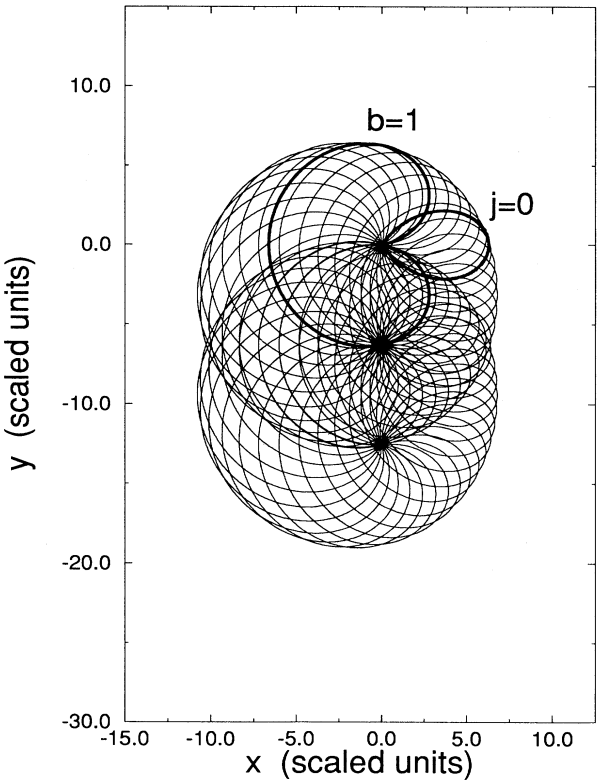

FIG. 5. The entire family of outgoing electron trajectories at a scaled energy $E = E^{(b1)}$, which is approximately 9.5. This is the energy of the first boundary orbit, and it is at this energy that the caustic comes tangent to the origin. One closed orbit has been created associated with $j = 1$ (the "heart-shaped" orbit). Notice that we have reduced the scale of the plot.

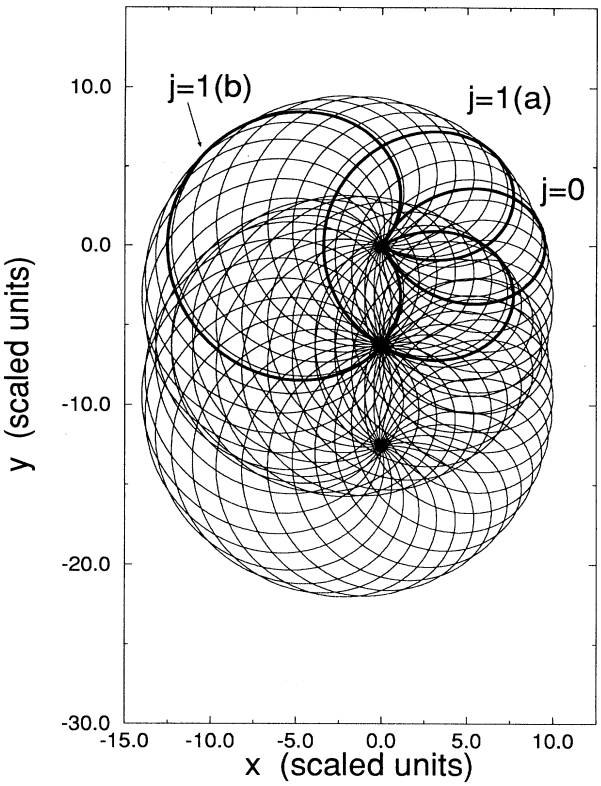

FIG. 6. Scaled energy $E = 18$. The caustic that was once touching the origin has moved upward. The boundary orbit has separated into two distinct orbits, both "heart-shaped," and associated with $j = 1(a)$ and $j = 1(b)$. At this energy there are three closed orbits. The $j = 0$ orbit continues to grow in size and becomes more circular.

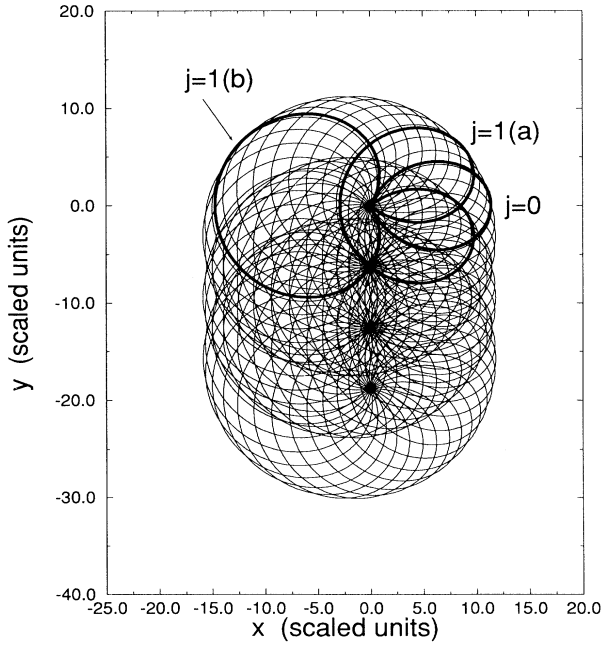

FIG. 7. Close to but below the second boundary energy in scaled units we see the second caustic rising towards the x axis.

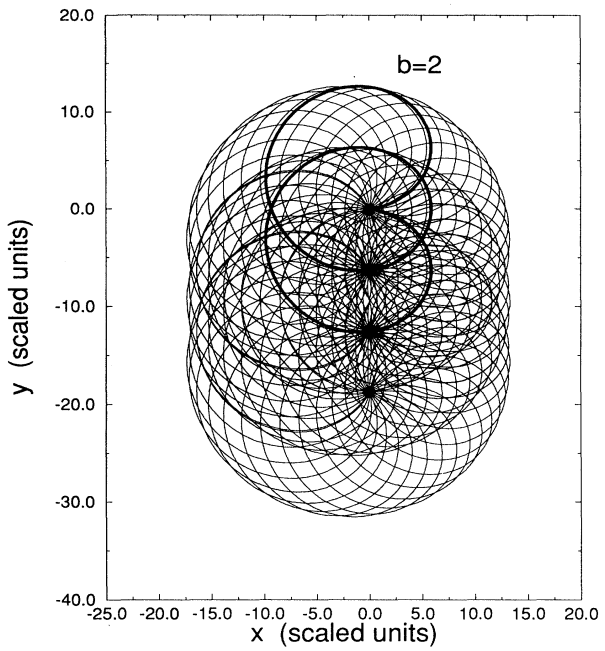

FIG. 8. At the second boundary energy ($E^{(b2)} \simeq 29.5$ scaled units), the second caustic has come tangent to the origin. A new closed orbit ($j=2$) is created, the "double-heart-shaped" orbit. We have omitted the $j=0$ and 1 orbits.

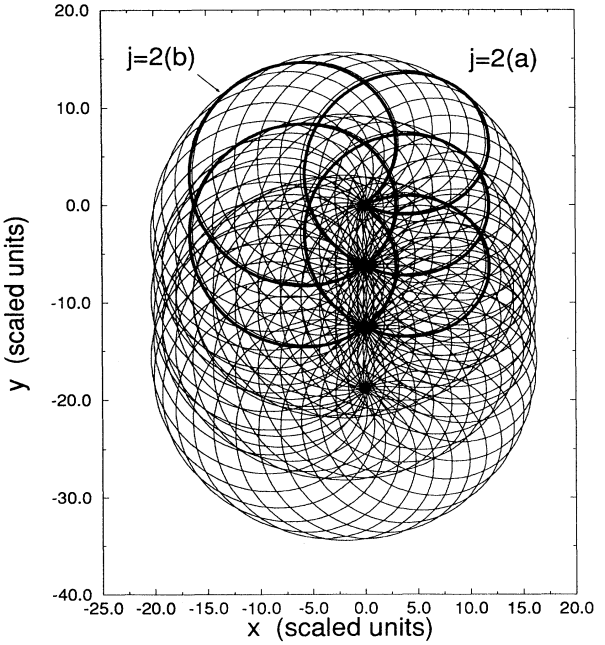

FIG. 9. For a scaled energy $E=42$, above the second boundary energy, the second caustic has risen above the x axis. The "double-heart-shaped" orbit of Fig. 8 splits into two distinct orbits, and are associated with $j=2(a)$ and $2(b)$. We omit here the $j=0$ and 1 orbits.

mechanics, we carry out the analysis in Hamiltonian form.

1. *Hamiltonian equations of motion*

Starting from Eq. (2.8), and defining the quantity

$$\varepsilon \equiv \frac{1}{2m_e}p_x^2 + \tfrac{1}{2}m_e\omega_B^2\left[x + \frac{1}{m_e\omega_B}\left[p_y + \frac{eF}{\omega_B}\right]\right]^2 , \tag{3.5}$$

the Hamiltonian may be expressed as

$$H = \varepsilon - \frac{eF}{m_e\omega_B}p_y + \frac{1}{2m_e}p_z^2 - \frac{1}{2m_e}\left[\frac{eF}{\omega_B}\right]^2 . \tag{3.6}$$

It is easy to show (for example, using Poisson brackets) that ε, p_y, and p_z are independently conserved.

Parameters in Eq. (3.6) can be eliminated by making the canonical scale change defined by Eqs. (3.1) and

$$\mathbf{p}' = \frac{\omega_B}{eF}\mathbf{p} , \tag{3.7a}$$

$$H' = \left[\frac{1}{m_e}\left[\frac{eF}{\omega_B}\right]^2\right]^{-1} H . \tag{3.7b}$$

In these variables, after dropping the primes, the Hamiltonian takes on the following uncomplicated form:

$$H = \tfrac{1}{2}p_x^2 + \tfrac{1}{2}[x + (p_y + 1)]^2 - p_y + \tfrac{1}{2}p_z^2 - \tfrac{1}{2} . \tag{3.8}$$

The fact that we are able to find a canonical scale transformation which completely removes the dependence of the Hamiltonian on the field strengths is somewhat surprising. The physical significance of this fact can be stated in the following ways: (1) The shapes of the trajectories do not depend on the electric and magnetic fields and the energy separately, but only upon the scaled energy, and this is given by Eq. (3.7b) above. (2) If we determine the trajectories (for all energies) for any one fixed value of electric and magnetic fields, then we have determined trajectories (for all energies) for any values of the electric and magnetic fields.

[Note that the new variables are all dimensionless. As a consequence, there are strange-looking combinations of variables in Eqs. (3.8), (3.15), and elsewhere. To check the units, one must go back to unprimed variables.]

As stated earlier, the initial conditions are that the electron begins at the origin, moving in any direction with fixed speed. The velocity is not proportional to the momentum; instead,

$$\begin{aligned} p_x(t) &= \dot{x}(t) , \\ p_y(t) &= \dot{y}(t) - x(t) = p_{y_0} , \\ p_z(t) &= p_{z_0} . \end{aligned} \tag{3.9}$$

The velocity in the y direction and the position in the x direction change in such a way as to keep the momentum p_y a constant. From the above, we can derive Eq. (3.2), and we can relate the phase angle φ to the initial values of the momenta,

$$\sin\varphi \equiv \frac{1}{\sqrt{2\varepsilon}}(p_{y_0}+1) ,$$
$$\cos\varphi \equiv \frac{p_{x_0}}{\sqrt{2\varepsilon}} . \tag{3.10}$$

2. *Initial conditions for closed orbits*

Let us now give quantitative conditions for returning orbits. As stated above, the trochoid must be prolate and $p_z=0$. From energy conservation we must have that $E=\varepsilon-p_{y_0}-\frac{1}{2}$. Since for returning orbits $x(t_{\rm ret})=0$, the possible return times are given by

$$t_{\rm ret}=-2\varphi+(2j+1)\pi . \tag{3.11}$$

We must also have $y(t_{\rm ret})=0$. This gives the condition relating the azimuthal angle φ to the circular energy ε:

$$\cos\varphi+\frac{1}{\sqrt{2\varepsilon}}\varphi-\frac{1}{\sqrt{2\varepsilon}}(j+\tfrac{1}{2})\pi=0 . \tag{3.12}$$

Equations (3.11) and (3.12) imply

$$t_{\rm ret}-2\sqrt{2\varepsilon}\cos\varphi=0 . \tag{3.13}$$

If the return time is to be positive, then $\cos\varphi$ must be defined on the interval from $\{-\pi/2,\pi/2\}$, where it is positive definite. This also means that it is the positive branch of the square root in $p_{x_0}=+[2\varepsilon-(p_{y_0}+1)^2]^{1/2}$ that we must take. The initial x component of momentum (and velocity) must be positive for returning orbits; i.e., the electron must begin its motion moving against the electric force.

Some additional manipulations reduce Eq. (3.12) to an equation involving only ε and the fixed total energy E. We eliminate φ and $t_{\rm ret}$ from the three equations (3.11)–(3.13) to obtain

$$[2\varepsilon-(\varepsilon-E_-)^2]^{1/2}-\cos^{-1}\left[\frac{(\varepsilon-E_-)}{\sqrt{2\varepsilon}}\right]=j\pi ,$$
$$L(\varepsilon)=j\pi , \tag{3.14}$$

where $E_-=E-\frac{1}{2}$ and $L(\varepsilon)$ is the left-hand side of (3.14).

Given the total energy E, this equation is used to determine the value of ε_j for which there is a closed orbit. Using energy conservation [Eq. (3.6)], we can determine the value for the momentum in the y direction (p_j) for that returning orbit. ε_j and p_j then determine the value of p_{x_0}. The initial conditions on the orbit are then known.

3. *Boundary orbits*

Let us now find how many closed orbits exist at each energy, and let us determine the boundary energies where new closed orbits appear. In Fig. 10 the left-hand side of Eq. (3.14) has been plotted at several values of the total energy E as a function of ε. The right-hand side has also been plotted for $j=1$. For a given energy E, the function on the left-hand has a single maximum. The right-hand side is a constant for fixed j. Notice that for all energies the maximum on the left-hand side is greater than zero, and therefore one solution exists for $j=0$ at all energies. At low values of E, the maximum of the left-hand side is less than π, and so no solutions exist for $j=1$. At large enough values of E, the function on the left has a maximum which is greater than π. In this case there are two roots to Eq. (3.14) having $j=1$, and hence two returning orbits, which are labeled $j=1(a)$ and $1(b)$.

There is another class of orbits which we call boundary orbits. At the energy $E^{(b1)}$, the curve representing the left-hand side is tangent to the line $j=1$. A new closed orbit is created at this energy. What are the boundary energies? They occur when the maximum of the left-hand side of Eq. (3.14) is equal to the right-hand side ($j\pi$). To find the maximum we differentiate with respect to ε, holding E fixed. For this purpose we define the function

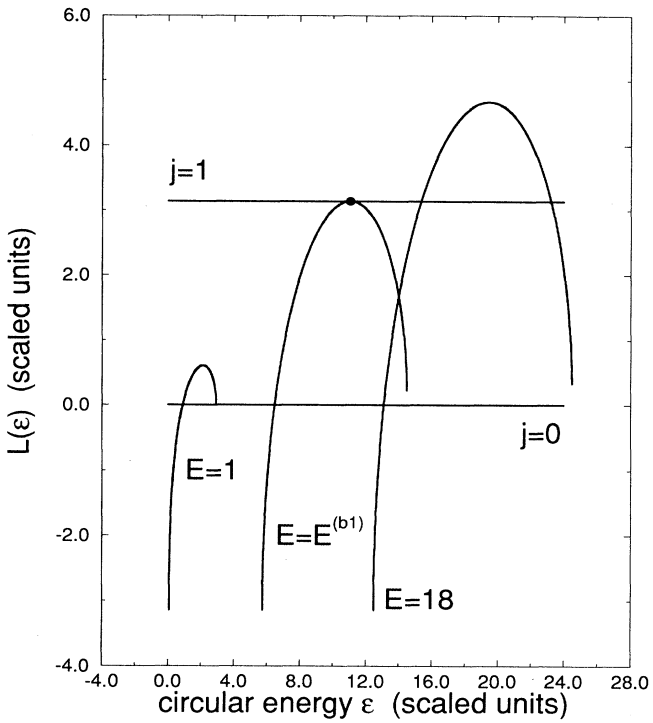

FIG. 10. Graphical solution to Eq. (3.14), the criterion for closed orbits. The curves represent the left-hand side (LHS) of Eq. (3.14), and the horizontal lines are the right-hand side (RHS). Intersections of the curves and lines are solutions of the equation. For all positive energies, a solution exists for Eq. (3.14) with $j=0$. For low scaled energies, the maximum of the LHS does not reach the value π, so there are no solutions for $j\geq 1$. For a scaled energy of $E=18$ there are two intersections of the curve with the line $j=1$, (RHS$=\pi$), and two solutions with $j=1$. These solutions have circular energies $\varepsilon_{1(a)}$ and $\varepsilon_{1(b)}$ which are the final conditions for two returning orbits. At boundary energies, such as when $E^{(b1)}\simeq 9.5$, the maximum of the LHS is tangent to the horizontal line defined by $j\pi$: this is where a caustic has come tangent to the origin. As the energy is increased from the boundary orbit energy, the boundary orbit associated with this tangency separates to form two distinct closed orbits.

$$p(\varepsilon)=\varepsilon-E_- \ , \tag{3.15}$$

and we find that the maximum occurs when

$$p(\varepsilon_b)=p_b=\frac{2}{1+\frac{1}{2\varepsilon_b}} \ . \tag{3.16}$$

We can substitute this value for $p(\varepsilon_b)$ into Eq. (3.14) and solve for the boundary energy ε_b numerically.

If ε_b is large, i.e., the total energy E is large, we can obtain a simple analytic expression for the magnitude of ε_b. In this approximation p_b is approximately equal to 2. We substitute this result back into (3.14) and expand out the square root and inverse cosine keeping terms to order $p_b/\sqrt{2\varepsilon_b}$; then solving for ε_b, we obtain

$$\varepsilon_b \simeq \tfrac{1}{2}[(b+\tfrac{1}{2})\pi]^2 \ . \tag{3.17}$$

Coming out of scaled variables, the approximate energies for the boundary orbits are given by (for large ε_b)

$$\varepsilon_b \simeq \frac{(eF/\omega_B)^2}{2m_e}[(b+\tfrac{1}{2})\pi]^2 \ , \tag{3.18}$$

and from energy conservation

$$E^{(b)}=\left[\frac{eF}{\omega_B}\right]^2\left[\frac{1}{2m_e}\right]\{[(b+\tfrac{1}{2})\pi]^2-3\} \ . \tag{3.19}$$

In Fig. 11 we graphically display the results of the last two sections concerning returning orbits and boundary orbits. Given an energy E, which is not the energy of a boundary orbit, there are $(2j_{\max}+1)$ returning orbits associated with that energy. There are two orbits which arise from solving Eq. (3.14) for each given j, from $j=1$ to $j_{\max}$, and one orbit for $j=0$. These orbits are labeled $j(a)$ and $j(b)$, where the inequality $\varepsilon_{j(a)} \le \varepsilon \le \varepsilon_{j(b)}$ holds.

As the total energy is increased, a boundary orbit is reached, and the number of returning orbits increases by one; i.e., there is now an even number of returning orbits. Upon the slightest increase in total energy, this new orbit separates into two orbits. The dashed curve in Fig. 11 was obtained by substituting Eq. (3.15) into Eq. (3.16), and calculating ε_b as a function of E. It represents the curve upon which new orbits will appear.

4. *The Jacobian*

The ratio of Jacobians appears in the semiclassical wave function as an amplitude $A_j(q)$, and represents the divergence of adjacent trajectories in time. As this ratio decreases, the probability density of the wave function is spread out over a larger area. Near caustics or foci, where trajectories converge on one another, the ratio of Jacobians increases and becomes infinite at the singular point. At these points the semiclassical approximation fails.

Here we will calculate the Jacobian by evaluating the expression

$$J(t)=\frac{\partial(x,y,z)}{\partial(t,\theta_{\text{out}},\phi_{\text{out}})} \ . \tag{3.20}$$

The coordinates $\{t,\theta_{\text{out}},\varphi_{\text{out}}\}$ are the coordinates for the family of trajectories, i.e., for the Lagrangian manifold. The intrinsic coordinates of the initial spherical surface, centered about the origin with radius r_{out}, are $\{t_0,\theta_{\text{out}},\varphi_{\text{out}}\}$, and t_0 is the same for any point on the sphere. They define the initial direction of motion of the electron. As the electron propagates into the external region, the symmetry is broken by the laboratory fields and a different set of coordinates becomes more convenient. In particular, $\{t,\sqrt{2\varepsilon},\varphi\}$ become the natural variables by which to express the motion. The intrinsic coordinates to the Lagrangian manifold are now taken to be $\{t_0,\sqrt{2\varepsilon},\varphi\}$, and again t_0 is the same for every point on the sphere. For this reason we reexpress the Jacobian in the following way:

$$J(t)=\frac{\partial(t,\sqrt{2\varepsilon},\varphi)}{\partial(t,\theta_{\text{out}},\phi_{\text{out}})}\frac{\partial(x,y,z)}{\partial(t,\sqrt{2\varepsilon},\varphi)} \ . \tag{3.21}$$

Writing out the derivatives explicitly, we have

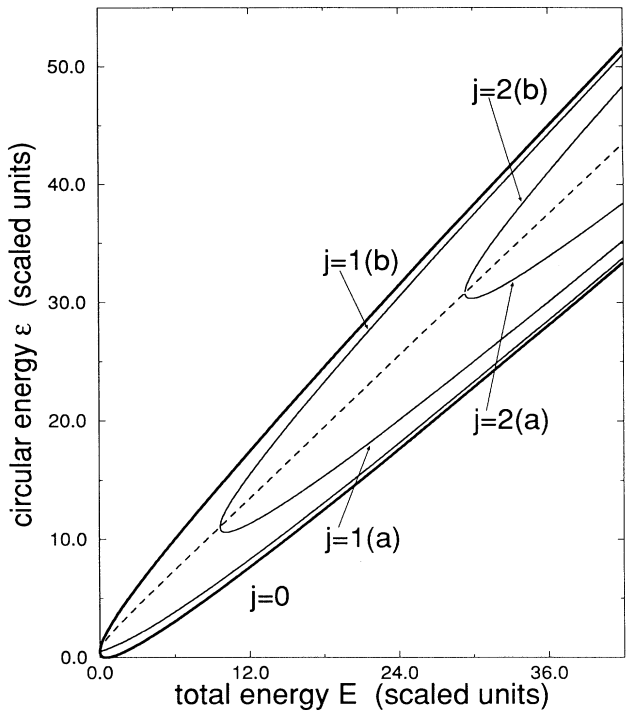

FIG. 11. The heavy curves are the maximum and minimum allowable values of the circular energy (ε) for a given E. For total energies less than approximately 9.5 there is one closed orbit. The value of $\varepsilon_{0(a)}$ as E varies is given by the curve labeled $j=0$. At an energy of approximately 9.5, the first boundary energy, we see the creation of a new orbit. This coincides with the first caustic coming tangent to the origin. As the total energy is increased, we see this orbit separate into the curves labeled $j=1(a)$ and $1(b)$. For energies above 9.5, but below $E^{(b2)} \simeq 29.5$, there are a total of three returning orbits. At the second boundary energy, the process repeats itself, with the addition of two new orbits labeled $j=2(a)$ and $2(b)$. The dashed curve is the curve upon which new orbits appear. In this figure we use scaled units.

$$J(t)=g(\varepsilon,\varphi)\begin{vmatrix} \frac{\partial x}{\partial t} & \frac{\partial x}{\partial\sqrt{2\varepsilon}} & \frac{\partial x}{\partial\varphi} \\ \frac{\partial y}{\partial t} & \frac{\partial y}{\partial\sqrt{2\varepsilon}} & \frac{\partial y}{\partial\varphi} \\ \frac{\partial z}{\partial t} & \frac{\partial z}{\partial\sqrt{2\varepsilon}} & \frac{\partial z}{\partial\varphi} \end{vmatrix}_{\det} . \tag{3.22}$$

The quantity $g(\varepsilon,\varphi)$ is the first determinant in Eq. (3.21). It is a geometrical factor and is independent of the time. Since the Jacobians always appear as ratios, this factor always cancels, so we are spared the necessity of evaluating $g(\varepsilon,\varphi)$. The determinant given in Eq. (3.22) is evaluated using Eqs. (3.2) and ten sheets of paper. The result is

$$J(t)=gt\frac{\sqrt{2\varepsilon}}{p_{z_0}}2\sin\frac{t}{2}\left[2(\varepsilon-p_{y_0}-\tfrac{1}{2})\cos\frac{t}{2} -2[2\varepsilon-(p_{y_0}+1)^2]^{1/2}\sin\frac{t}{2}\right] . \tag{3.23}$$

This is the Jacobian for any trajectory at any arbitrary time (the trajectory is not necessarily a closed orbit).

For returning orbits the momentum in the z direction is zero. If $t=t_0$ (initial time) or $t=t_{\rm ret}$ (return time), then x is small, and with this in mind we write

$$\tfrac{1}{2}(\hbar k)^2=\varepsilon_j-p_{y_0}-\tfrac{1}{2} . \tag{3.24}$$

[Here the quantity $\hbar k$ is understood to be the dimensionless "primed" initial kinetic momentum, transformed from its initial form by Eq. (3.7a).] Equation (3.24) allows us to rewrite the Jacobian in the following way:

$$J(t)=gt\frac{\sqrt{2\varepsilon_j}}{p_{z_0}}2\sin\frac{t}{2}\left[(\hbar k)^2\cos\frac{t}{2} -2[2\varepsilon_j-(p_{y_0}+1)^2]^{1/2}\sin\frac{t}{2}\right] . \tag{3.25}$$

Equation (3.25) is the Jacobian evaluated at either $t=t_0$ or $t=t_{\rm ret}$.

C. The ratio of Jacobians and $A(q)$

Let us construct the ratio of Jacobians for $t=t_0$ and $t=t_{\rm ret}$. Consider the Jacobian when $t=t_0$ with t_0 small. In this case, expanding the trigonometric functions of Eq. (3.25) and keeping only the lowest order,

$$J(t_0)=g\frac{\sqrt{2\varepsilon_j}}{p_{z_0}}t_0^2(\hbar k)^2 . \tag{3.26}$$

If $t=t_{\rm ret}$ we have from Eq. (3.11) that $t_{\rm ret}=-2\varphi+(2j+1)\pi$, and so

$$\cos\frac{t_{\rm ret}}{2}=(-1)^j\sin\varphi,\quad \sin\frac{t_{\rm ret}}{2}=(-1)^j\cos\varphi . \tag{3.27}$$

Additionally, from the remark below Eq. (3.13) we have the expression $t_{\rm ret}=2[2\varepsilon_j-(p_j+1)^2]^{1/2}$. Substituting in the definitions for $\sin(\varphi)$ and $\cos(\varphi)$ we have that the Jacobian at $t=t_{\rm ret}$ is given by

$$J(t_{\rm ret})=g\frac{(2\varepsilon_j)^2}{p_{z_0}}4\left[1-\left[\frac{p_j+1}{\sqrt{2\varepsilon_j}}\right]^2\right] \times\left[\frac{p_j+1}{\sqrt{2\varepsilon_j}}\left[1+\frac{1}{2\varepsilon_j}\right]-\frac{2}{\sqrt{2\varepsilon_j}}\right] . \tag{3.28}$$

Using Eqs. (3.26) and (3.28), we have that the ratio of Jacobians, for returning orbits, is given by

$$\frac{J(t_0)}{J(t_{\rm ret})}=\frac{\tilde{\nu}_j^2}{(eF/\omega_B)^2}\frac{\tilde{\nu}_j\omega_B^2t_0^2(\hbar k)^2}{4(1-\tilde{\nu}_j^2)[\nu_j(1+\tilde{\nu}_j^2)-2\tilde{\nu}_j]} , \tag{3.29}$$

and we have made use of the following dimensionless variables:

$$\tilde{\nu}_j\equiv\frac{(eF/\omega_B)}{\sqrt{2m_e\varepsilon_j}} ,\qquad \nu_j\equiv\frac{1}{\sqrt{2m_e\varepsilon_j}}\left[p_j+\frac{eF}{\omega_B}\right] . \tag{3.30}$$

The quantity $\tilde{\nu}_j$ is the drift speed divided by the circular speed, and ν_j is the initial y component of velocity in the drift frame divided by the circular speed. We have also come out of scaled variables.

There is no simple interpretation to Eq. (3.29). We repeat that this ratio gives the classical density at the origin for a returning orbit, which is related to the amplitude of the returning quantum wave.

D. The Maslov index

Caustics and foci are singular points where the Jacobian goes to zero and hence the coefficient $A(q)$ goes to infinity. As the electron passes through either a caustic or focus, the Maslov index increases by one.

From the time dependence outside the brackets in the Jacobian of Eq. (3.25), we see that the function goes to zero when $t=2k\pi$, with t less than or equal to $t_{\rm ret}$. As we already learned, $t=2k\pi$ is a multiple of the cyclotron time, and the electron is passing through a focus located along the negative y axis. The Jacobian is also zero when

$$\tan\frac{t}{2}=\frac{\varepsilon-p_{y_0}-\frac{1}{2}}{[2\varepsilon-(p_{y_0}+1)^2]^{1/2}} , \tag{3.31}$$

and these are the times when the electron passes through a caustic.

Given the total energy E, there are two closed orbits for each j of Eq. (3.14). The circular energies of these orbits are designated by the variables $\varepsilon_{j(a)}$ and $\varepsilon_{j(b)}$. An important question to ask is: given $\varepsilon_{j(a)}$ and $\varepsilon_{j(b)}$, how many caustics and foci has the electron passed through upon its return to the origin? Equation (3.31) helps to answer this question.

The return time for the jth closed orbit must be greater than $2j\pi$ but less than $(2j+2)\pi$. Using the dimensionless

parameters defined by Eq. (3.30), we rewrite Eq. (3.16) in the following way:

$$\nu_b = \frac{2\tilde{\nu}_b}{1+\tilde{\nu}_b^2} \ . \tag{3.32}$$

As the total energy E increases, the boundary orbit separates into two orbits having circular energies $\varepsilon_{j(a)}$ and $\varepsilon_{j(b)}$. These energies diverge from the curve defined by Eq. (3.32), with one moving above and the other dropping below. We have

$$\nu_{j(a)} \leq \frac{2\tilde{\nu}_b}{1+\tilde{\nu}_b^2}, \quad \nu_{j(b)} \geq \frac{2\tilde{\nu}_b}{1+\tilde{\nu}_b^2} \ , \tag{3.33}$$

and therefore $\varphi_{j(a)} \leq \varphi_{j(b)}$. Consequently, $t_{j(a)} \geq t_{j(b)}$.

From the preceding arguments, $2j\pi < t_{j(b)} \leq t_{j(a)} < (2j+2)\pi$. We are also able to conclude that the orbits labeled $j(a)$ pass through $(2j+1)$ caustics and foci, while orbits labeled $j(b)$ pass through $2j$ caustics and foci. This result is consistent with the pictures of the trajectories (Figs. 3–9).

E. The classical action

The classical action $S(q)$ appears in the phase of the semiclassical wave function and is defined in Sec. II, Eq. (2.27). The action is equal to

$$S(\mathbf{q}) = \int_{\mathbf{q}_0}^{\mathbf{q}} \mathbf{p}\cdot d\mathbf{q} \ , \qquad S(\mathbf{q}) = \int_{\mathbf{q}_0}^{\mathbf{q}} \mathbf{p}\cdot\frac{d\mathbf{q}}{dt}dt \ . \tag{3.34}$$

S_0 is an arbitrary phase factor which is taken to be zero. The integrals are evaluated using Eqs. (3.2) and (3.9). A long but straightforward analysis gives

$$S(E) \equiv S(t_{\rm ret}) = -\frac{1}{m_e\omega_B}\left[\frac{eF}{\omega_B}\right]^2 \frac{1}{\tilde{\nu}_j^2}(1-\nu_j^2)^{1/2}\left[\nu_j - \frac{1}{\tilde{\nu}_j}\right] . \tag{3.35}$$

Again, there is no simple "intuitive" explanation. This formula gives the phase of the returning wave. We also note the theorem from classical mechanics which asserts that $\partial S(E)/\partial E = t_{\rm ret}$, so S is a monotonic function of E.

IV. THE PHOTODETACHMENT CROSS SECTION

Now we combine the results of the preceding sections to obtain the photodetachment cross section in crossed fields. Let us summarize the important previous results:

(i) The photodetachment cross section is given by Eqs. (2.3)–(2.5); it is the no-field cross section plus a sum of oscillatory terms. Each oscillatory term arises from a closed orbit.

(ii) At low energies there is one closed orbit, and at each of a set of boundary energies a new closed orbit is created. Above the boundary energy the orbit splits into two. The boundary energies are given approximately by Eq. (3.19). One can also use numerical methods to calculate the exact value of the boundary energies. Using Eqs. (3.15) and (3.16), one solves for ε_b in terms of $E^{(b)}$. Substituting this result into Eq. (3.14), one can numerically solve for the boundary energies.

(iii) Each closed orbit is labeled by an index $j(a)$ or $j(b)$. It is characterized by the parameter ε, which represents the circular kinetic energy of the electron on that orbit. The value of ε is obtained by numerical solution of Eq. (3.14); by convention $\varepsilon_{j(a)} \leq \varepsilon_{j(b)}$.

(iv) The ratio of Jacobians is given by Eq. (3.29).

(v) The Maslov index for the $j(a)$ orbit is $2j+1$, while for the $j(b)$ orbit it is $2j$.

(vi) The classical action on each orbit is given by Eq. (3.35), where we have made use of the parameters $\tilde{\nu}_j$ and ν_j that are defined in Eq. (3.30).

(vii) For H^- the radial dipole integral was given in Eq. (2.17), and the angular distribution of outgoing waves was given in Eqs. (2.12), assuming linearly polarized light on the x, y, or z axis.

Now we combine these results into a single formula for the oscillatory part of the cross section:

$$\sigma_{\rm ret} = \sigma_0 \sum_j \left[\frac{6m_e\omega_B}{(eF/\omega_B)}\right]\frac{\pi}{k}\left|\frac{\tilde{\nu}_j^3}{(1-\nu_j^2)[\nu_j(1+\tilde{\nu}_j^2)-2\tilde{\nu}_j]}\right|^{1/2} [\chi(\theta_{\rm out}^j,\phi_{\rm out}^j)\chi^*(\theta_{\rm ret}^j,\phi_{\rm ret}^j)] \times \sin\left[\frac{1}{\hbar m_e\omega_B}\left[\frac{eF}{\omega_B}\right]^2\frac{1}{\tilde{\nu}_j^2}(1-\nu_j^2)^{1/2}\left[\nu_j-\frac{1}{\tilde{\nu}_j}\right]+\mu_j\frac{\pi}{2}\right] . \tag{4.1}$$

For the angular factor, the geometry of the returning orbits requires that $\theta_{\rm out}=\theta_{\rm ret}=\pi/2$ and $\phi_{\rm out}=-\phi_{\rm ret}$. This allows us to write for various linear polarizations

$$\chi_x(\theta_{\rm out},\phi_{\rm out})\chi_x^*(\theta_{\rm ret},\phi_{\rm ret}) = \frac{1}{4\pi}\cos^2(\phi_{\rm out}) \ ,$$
$$\chi_y(\theta_{\rm out},\phi_{\rm out})\chi_y^*(\theta_{\rm ret},\phi_{\rm ret}) = -\frac{1}{4\pi}\sin^2(\phi_{\rm out}) \ , \tag{4.2}$$
$$\chi_z(\theta_{\rm out},\phi_{\rm out})\chi_z^*(\theta_{\rm ret},\phi_{\rm ret}) = 0 \ .$$

With z-polarized light, there is no outgoing wave in the x-y plane, so the returning orbits have no effect, and the cross section should have no oscillations.

The angle $\phi_{\rm out}$ is the outgoing direction of the orbit in the rest frame of the atom; through Eqs. (3.9) this can be expressed in terms of p_{y_0}, and then reexpressed in the parameters $\tilde{\nu}_j$ and ν_j:

$$\chi_x(\theta_{\rm out},\phi_{\rm out})\chi_x^*(\theta_{\rm ret},\phi_{\rm ret}) = \frac{1}{4\pi}\left[\frac{eF}{\omega_B}\right]^2 \times \frac{1}{(\hbar k)^2}\frac{1}{\tilde{\nu}_j^2}(1-\nu_j^2) \ ,$$
$$\chi_y(\theta_{\rm out},\phi_{\rm out})\chi_y^*(\theta_{\rm ret},\phi_{\rm ret}) = -\frac{1}{4\pi}\left[\frac{eF}{\omega_B}\right]^2 \times \frac{1}{(\hbar k)^2}\frac{1}{\tilde{\nu}_j^2}\frac{(\nu_j-\tilde{\nu}_j)^2}{(1-\nu_j^2)^{1/2}} \ . \tag{4.3}$$

Hence we obtain the recurrence amplitudes

$$C_j^x(E)=\sigma_0\left[\frac{3}{2}\frac{m_e\hbar eF}{(\hbar k)^3}\frac{1}{\tilde{\nu}_j}\right]\left|\frac{\tilde{\nu}_j(1-\nu_j^2)}{\nu_j(1+\tilde{\nu}_j^2)-2\tilde{\nu}_j}\right|^{1/2}, \quad (4.4)$$

$$C_j^y(E)=-\sigma_0\left[\frac{3}{2}\frac{m_e\hbar eF}{(\hbar k)^3}\frac{1}{\tilde{\nu}_j}\right]\left|\frac{\tilde{\nu}_j}{\nu_j(1+\tilde{\nu}_j^2)-2\tilde{\nu}_j}\right|^{1/2} \times\frac{(\nu_j-\tilde{\nu}_j)^2}{(1-\nu_j^2)^{1/2}}, \quad (4.5)$$

$$C_j^z(E)=0. \quad (4.6)$$

In Figs. 12(a) and 13(a) we show a numerical calculation, derived from a purely-quantum-mechanical treatment of the photodetachment cross section. Such treatment was first developed by Fabrikant [7] and is further discussed in the following paper. The range of E is from 0.0 to 4.0×10^{-5} a.u. The light is linearly polarized, and we have chosen the magnetic field strength to be $\frac{3}{5}$ T, and the electric field strength to be 18 V/cm. We see that the cross sections are smooth, rising functions (no-field cross section), superposed upon which are oscillations. The curves are well behaved with no divergences. We wish to compare this result to the result obtained from the semiclassical analysis.

To calculate the semiclassical cross section for the parameters shown in Fig. 12(a) [or Fig. 13(a)] we use the following algorithm. For a given energy E we first determine the number of returning orbits for that energy. Us-

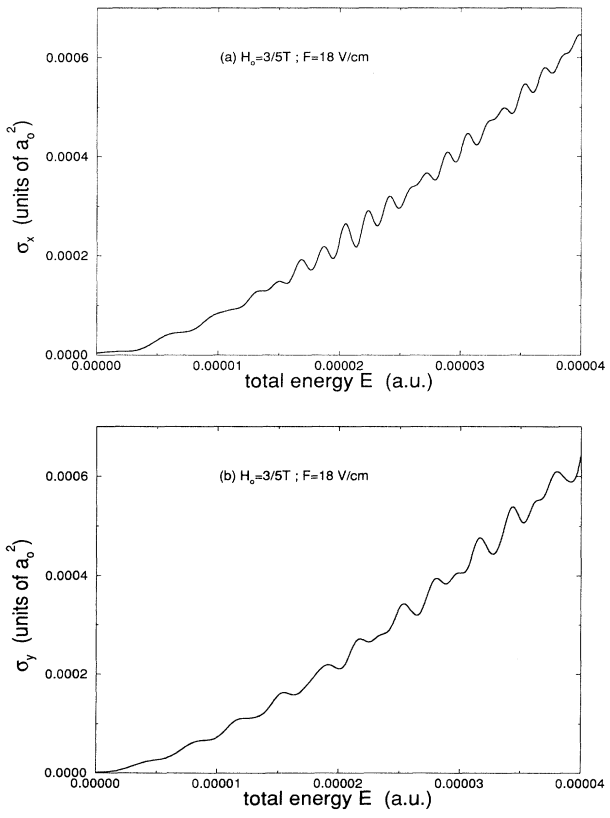

FIG. 12. Photodetachment cross section calculated from the quantum-mechanical method discussed in the following paper. The cross section is a smooth, rising function of energy (the no-field cross section), superposed upon which are oscillations. The oscillations are small, but near threshold they are a substantial fraction of the background. (a) x-polarized light. (b) y-polarized light.

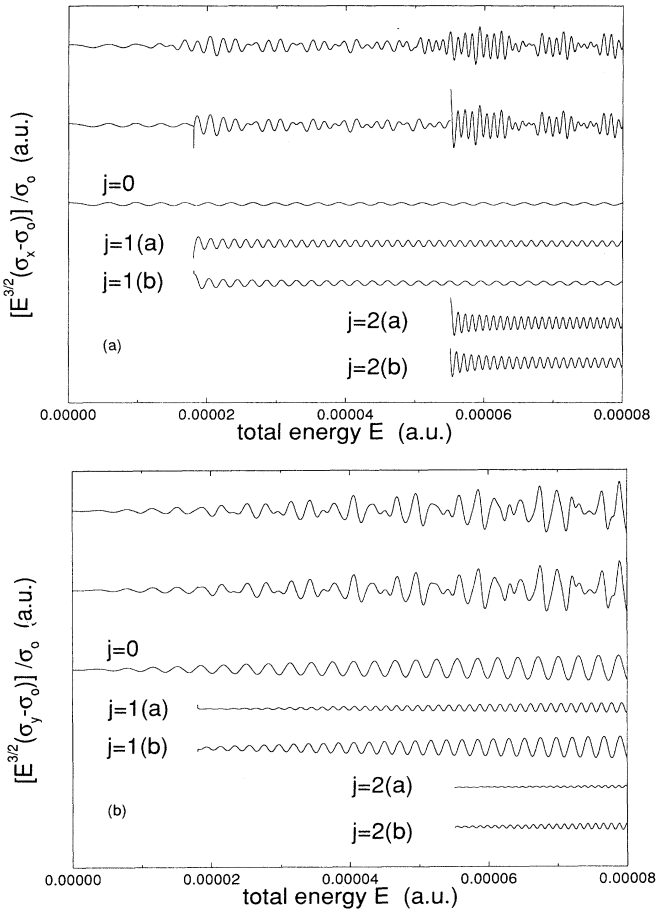

FIG. 13. In the top graph we redisplay Fig. 12, the quantum-mechanical oscillations. We have subtracted out the no-field cross section and multiplied by a scaling factor. The graph immediately below this is the semiclassical oscillations derived from Eq. (4.8). Oscillatory contributions from each orbit are displayed separately. There is a very nice agreement between the two approaches. For energies less than the first-boundary-orbit energy, the sum in Eq. (4.8) involves only one term, $j=0(a)$, associated with the balloon-shaped orbit. For energies between the first- and second-boundary-orbit energies, there are three returning orbits, and hence three terms to the sum of Eq. (4.8) [$j=0(a)$, $j=1(a)$, and $j=1(b)$]. The $j=1$ terms are associated with the heart-shaped orbits in Fig. 6. For energies above the second boundary energy and below 8.0×10^{-5} there are five orbits. The two new orbits are associated with the double-heart-shaped orbits of Fig. 9. Notice the singularity at both the first and second boundary orbits in the semiclassical oscillations. For x-polarized light (a), each oscillation decreases with increasing energy, while for y-polarized light (b), each oscillation increases. End points of orbits move from the x axis to the y axis.

ing the scaling transformation Eq. (3.7b), we have that the total scaled energy is given by

$$E' = \left[\frac{1}{m_e} \left[\frac{eF}{\omega_B} \right]^2 \right]^{-1} E \ . \tag{4.7}$$

From Table I, or for the higher energies, the approximation given by Eq. (3.19), we can determine the number of closed orbits. For example, with the fields as chosen above, and taking $E = 4.0 \times 10^{-5}$ a.u., the total scaled energy is approximately 21.8. From Table I we see that this scaled energy lies between the first and second boundary energies. For scaled atomic energies less than 10.133 there is one closed orbit (see Fig. 3 or Fig. 4), and hence one term in the sum of Eq. (4.1). For energies between 10.133 and 29.85 there is a total of three closed orbits, and so at the energy of 4.0×10^{-5} a.u. there will be three terms associated with the sum of Eq. (4.1).

Second, for a given E we calculate ε_j for each returning orbit by solving Eq. (3.14). Therefore, if we consider $E = 4.0 \times 10^{-5}$ a.u., we will need to determine the various values for $\varepsilon_{j=0(a)}$, $\varepsilon_{j=1(a)}$, and $\varepsilon_{j=1(b)}$. With this done we use Eq. (3.16) to calculate p_j, and therefore evaluate the two ratios $\tilde{\nu}_j$ and ν_j [Eq. (3.30)]. Using these values for $\tilde{\nu}_j$ and ν_j we obtain a value for the cross section at the energy E by evaluating Eq. (4.1), using Eqs. (4.3) and (4.4).

It is useful to write the photodetachment cross section, for x-polarized light, in the following manner:

$$(E)^{3/2} \left[\frac{\sigma_x - \sigma_0}{\sigma_0} \right] = \frac{1}{\sigma_0} \sum_j C_j^x(E) \sin[\Phi_j(E)] \ . \tag{4.8}$$

A similar equation holds for y-polarized light. We have subtracted out the no-field cross section, leaving only the oscillatory part of the spectrum. Dividing by σ_0 and multiplying by the factor $(E)^{3/2}$ merely changes the amplitude of the oscillations. Following the algorithm described above, the right-hand side of Eq. (4.8) was calculated for the range of atomic energies $0.0-8.0 \times 10^{-5}$ a.u., giving the semiclassical results in Fig. 13.

The topmost graph shows the oscillations obtained from the quantum-mechanical calculation shown in Fig. 12(a). The semiclassical oscillations are displayed immediately below this. For energies less than the first boundary energy, the oscillations of the semiclassical result are due to the single closed orbit $j=0$, the balloon-shaped orbit shown in Fig. 3 or 4. For energies between the first and second boundary energies, two additional orbits contribute, the heart-shaped orbits of Fig. 6. These two orbits have similar return times, and the two resulting oscillations produce beats.

For energies above the second boundary energy, two additional orbits have appeared (Fig. 9), again the oscillations produce beats, and again they are plainly visible in the quantum calculation. At the boundary energies, the semiclassical approximation diverges, because a caustic has touched the atom.

Just below each boundary a caustic is close to the atom, but the atom is on the classically forbidden side of the caustic. The new, about-to-be-created returning orbits carry returning waves close to the atom, but the orbits pass slightly below the atom, and the waves miss. However, the waves spill over slightly into the classically forbidden region, so these orbits produce small oscillations just below their boundary energy. This effect is plainly visible in the quantum oscillations. A uniform semiclassical calculation (using an Airy function near the caustic) can also describe this.

The amplitude of the oscillations for x-polarized light are greatest near the boundary energy and then decrease with increasing energy. This effect is seen most clearly in the decreasing amplitude of the oscillations of the $j=2(a)$ and $2(b)$ orbits shown in the lower part of Fig. 12(b). This can be explained in the following way. The coefficient for x-polarized light is proportional to $\cos^2(\phi_{\text{out}})$. When the total energy is at one of the boundary energies, ϕ_{out} is at a minimum for that orbit. The trajectory of the boundary orbit leaves and returns primarily oriented in the x direction, and consequently the amplitude of the oscillations is at a maximum. As the total energy increases, ϕ_{out} increases and the amplitude decreases: the returning trajectory is aligning itself with the y axis. (Compare Figs. 3 and 6.)

For y-polarized light, the opposite happens [see Figs. 13(a) and 13(b)]. The angular factor is proportional to $\sin^2(\phi_{\text{out}})$, so the amplitude of the oscillations increases with increasing energy.

The results for the semiclassical analysis can be used for other values of field strengths as well. Specifically, if we change ω_B and F in such a way as to keep the drift velocity (F/ω_B) constant, then since the scaled energy is fixed, from Sec. III we know that the number of returning orbits in the interval of E will not change. The amplitude of the oscillations will scale like the electric-field strength F, while their wavelength will scale like ω_B. In Sec. III we found that it was possible to scale the Hamiltonian in such a way that the dependence upon the fields was eliminated. It is this fact which allows us to use one set of parameters to describe results for other field strengths.

Taking this a step further, it would be useful to consider the oscillations of Eq. (4.8) as a function of the scaled variables defined in Sec. III. The cross section becomes a function of the total scaled energy, the magnetic-field strength (proportional to ω_B), and the electric-field strength F. It is true that the coefficient and phase of the

TABLE I. The total energy and circular energy for a given boundary orbit are listed here. The units of energy are the scaled units as defined by Eq. (4.7).

Boundary orbit	$\hat{E}^{(b)}$	$\hat{\varepsilon}^{(b)}$
1	9.633	11.05
2	29.35	30.82
3	58.96	60.44
4	98.43	99.92
5	147.8	149.3
6	207.0	208.5
7	276.1	277.6
8	355.0	356.5
9	443.9	445.4
10	542.6	544.1

semiclassical cross section depend upon the parameters in a complicated way; however, if we hold the total scaled energy fixed, the number of returning orbits does not change as we vary the field strengths, and the values of $\tilde{\nu}_j$ and ν_j do not change. Therefore, matters are quite simplified. In particular, each term of the sum of Eq. (4.8) is an amplitude times a pure sinusoidal oscillation, whose Fourier transform is a single peak located at the return time for that particular orbit.

The scaled energy can be held fixed in a number of ways. We might consider fixing the total atomic energy, and varying both ω_B and F in such a way as to keep the drift velocity (F/ω_B) a constant. Then if we plot the left-hand side of Eq. (4.8) versus $1/\omega_B$, the result will be a sum of pure sinusoidal oscillations with an amplitude which scales like the electric-field strength (F).

A second possibility is to hold the electric field constant, varying both the total atomic energy and the magnetic field in such a way that the scaled energy remains fixed. If we plot the left-hand side of Eq. (4.8) with respect to $(1/\omega_B)^3$, we will again obtain pure sinusoidal oscillations. The amplitude of the oscillations is a constant and is proportional to the electric-field strength. The wavelength is proportional to the constant $(1/F)^2$.

A final alternative is to hold the magnetic field fixed while varying the total atomic energy and the electric-field strength in order to maintain a fixed scaled energy. Plotting the left-hand side of Eq. (4.8) as a function of F^2 will give a pure sinusoidal oscillation. The amplitude of the oscillations scales like F, while the wavelength is proportional to the constant $(1/\omega_B)^3$. Finally, we note that although the oscillations are small, they might be made detectable by repeated rotation of the plane of polarization, observing $(\sigma_x-\sigma_z)$, $(\sigma_y-\sigma_z)$, or best of all $(\sigma_x-\sigma_y)$.

ACKNOWLEDGMENTS

This work was supported by the Jeffress Foundation, by the Office of Naval Research, and by the National Science Foundation through grants to the College of William and Mary and to the Institute for Theoretical Atomic and Molecular Physics. The hospitality of the Institute is gratefully acknowledged.

*Present address: Department of Chemistry, West Virginia University, Morgantown, WV 26506.

†1992–93 address: MS14, Harvard-Smithsonian Center for Astrophysics, 60 Garden Street, Cambridge, MA 02138.

[1] W. R. S. Garton and F. S. Tomkins, Astrophys. J. **158**, 839 (1969).

[2] A. Holle, J. Main, G. Wiebusch, H. Rottke, and K. H. Welge, Phys. Rev. Lett. **61**, 161 (1988); Chon-ho Iu, G. R. Welch, M. M. Kash, Long Hsu, and D. Kleppner, *ibid.* **63**, 1133 (1989).

[3] M. L. Du and J. B. Delos, Phys. Rev. A **38**, 1913 (1988); **38**, 1896 (1988).

[4] D. Delande, A. Bommier, and J. C. Gay, Phys. Rev. Lett. **66**, 141 (1991); C.-h. Iu, G. T. Welch, M. M. Kash, D. Kleppner, D. Delande, and J. C. Gay, *ibid.* **66**, 145 (1991); P. F. O'Mahony and F. Mota-Furtado, Comm. At. Mol. Phys. **25**, 309 (1991); Q. Wang and C. H. Greene, Phys. Rev. A **44**, 1874 (1991); **44**, 7448 (1991); S. Watanabe, Y. Hosoda, and H. Komine, *ibid.* **46**, 2693 (1992).

[5] H. C. Bryant, A. Mohagheghi, J. E. Stewart, J. B. Donahue, C. R. Quick, R. A. Reeder, V. Yuan, C. E. Hummer, W. W. Smith, S. Cohen, W. P. Reinhardt, and L. Overman, Phys. Rev. Lett. **58**, 2412 (1987).

[6] Yu. N. Demkov and G. F. Drukarev, Zh. Eksp. Teor. Fiz. **47**, 918 (1964) [Sov. Phys.—JETP **20**, 614 (1965)]; M. L. Du and J. B. Delos, Phys. Rev. A **38**, 5608 (1988); W. P. Reinhardt, in *Atomic Excitation and Recombination in External Fields,* edited by M. H. Nafeh and C. W. Clark (Gordon and Breach, New York, 1985), p. 85; V. Z. Slonim and F. I. Dalidchik, Zh. Eksp. Teor. Fiz. **71**, 2057 (1976) [Sov. Phys.—JETP **44**, 1081 (1976)]; H.-Y. Wong, A. R. P. Rau, and C. H. Greene, Phys. Rev. A **37**, 2393 (1988).

[7] M. L. Du, Phys. Rev. A **40**, 1330 (1989).

[8] I. I. Fabrikant, Phys. Rev. A **43**, 258 (1991).

[9] I. S. Gradshetyn and I. M. Ryzhik, *Table of Integrals, Series, and Products,* Corrected and Enlarged Edition (Academic, New York, 1980), p. 711, Eq. 6.621.1(c).

[10] John David Jackson, *Classical Electrodynamics,* 2nd ed. (Wiley, New York, 1975), pp. 582–584.